Composites Part B 255 (2023) 110606

Contents lists available at ScienceDirect

Composites Part B

journal homepage: www.elsevier.com/locate/compositesb

Experimental study of post-buckled single-stringer composite specimens under fatigue loads with different load levels and load ratios

Javier Paz, Antonio Raimondo, Chiara Bisagni *

Delft University of Technology, Faculty of Aerospace Engineering, Delft, the Netherlands

ARTICLE INFO

Handling Editor: Prof. Ole Thomsen

Keywords:
Composite structures
Post-buckling
Fatigue
Delamination
Load ratio
Experimental tests

ABSTRACT

This study aims at better understanding the damage tolerance of stiffened composite panels subjected to fatigue loads in the post-buckling regime. Ten single-stringer hat-stiffened specimens with an initial delamination between the skin and the stringer foot were manufactured, and then tested under quasi-static and fatigue loads in post-buckling conditions, with different load levels and load ratios. The tests were monitored with digital image correlation and an ultrasonic system, providing data on the displacements, strains, and extension of the delamination length. The quasi-static results showed that the delamination onset, when the initial delamination begins propagating, occurred at loads over twice the buckling load, while collapse occurred for values almost 20% higher than the delamination onset. During fatigue testing at load levels below the delamination onset, the specimens were able to sustain 150000 cycles and then, when tested statically after fatigue, the average load at collapse was reduced by less than 10% with respect to the quasi-static benchmark. When the maximum load during fatigue was increased to 5% over the delamination onset load, the specimens still withstood between 8000 and 16500 cycles before collapse, depending on the load ratio. It was also seen that for tests at the same load level, the specimens with high load ratio had a slower damage propagation.

1. Introduction

Carbon fiber-reinforced composites are ever more used by the aerospace industry, aiming for more efficient structures with lower mass, higher strength, and an increased lifespan with respect to metallic counterparts. Stiffened panels are typical aerospace components and can carry loads higher than buckling loads [1,2], but today they are in most cases designed following a conservative no-buckling approach due to the difficulties in controlling and predicting the highly non-linear behavior and the complex damage mechanisms [3]. However, if the behavior of these panels in post-buckling conditions could be fully understood throughout their service life, much lighter and efficient designs could be achieved.

Delamination, and in particular skin-stringer separation, is a common cause of failure in composite stiffened panels [4]. When the skin begins to buckle, significant interface stresses between skin and stringers appear due to the inherent mismatch in their flexural stiffness, thus making this type of damage among the most critical and difficult to predict [5]. Furthermore, it has been shown that the presence of an initial delamination or impact indentation can lead to an excessive growth of the damage and the premature collapse of these structures [6,7]. The prediction of the collapse needs to account for the interaction of the post-buckling displacement with different failure modes, such as intralaminar damage or skin-stringer separation [8].

When components are subjected to cyclic loads, fatigue life and delamination growth are usually characterized using the Paris law [9] that relates the growth rate with the ratio between the minimum and maximum stress values at the crack tip, known as the local stress ratio. However, for these stiffened structures the local stress ratio at the delamination front is not only different from the applied load ratio, but it changes as the delamination propagates due to the interaction between the geometric non-linearities of the response, the different possible damage modes, and the accumulation of cyclic damage [10].

The effects of the stress ratio on the fatigue life of composites have been thoroughly assessed on coupons and simplified specimens that represent the skin/stringer bond, both numerically [11–13] and experimentally [14,15]. However, in the case of composite stiffened panels most research focused on the effect of the load ratio and their fatigue life has been studied solely from the numerical approach [16], where the use of numerical tools as cohesive-zone model methods [17] or the virtual

* Corresponding author.
E-mail address: C.Bisagni@tudelft.nl (C. Bisagni).

https://doi.org/10.1016/j.compositesb.2023.110606
Received 9 December 2022; Received in revised form 31 January 2023; Accepted 9 February 2023
Available online 11 February 2023

crack-closure technique [18] have proved crucial to accurately evaluate local fracture parameters in non-linear three-dimensional structural cases. A few authors have experimentally investigated and reported the buckling and post-buckling behavior of composite stiffened structures under quasi-static and fatigue compressive loads [19–21], although these test campaigns only consider one combination of load level and load ratio. Recent experimental works include research on the propagation of an artificial delamination or impact damage in post-buckling conditions of hat-stiffened [22], T-stiffened [23], I-stiffened [24], and J-stiffened panels [25]; highlighting the strive for gaining further knowledge on this topic to increase the component structural efficiency.

In the case of hat-stiffened composite structures, experimental test campaigns were carried out in Refs. [26–28] to study the damage tolerance and fatigue life of components featuring either an initial delamination or indentation damage. Single-stringer specimens were subjected to cyclic compressive loads between pre- and post-buckling conditions, showing that these panels could be safely taken into the post-buckling regime repeatedly, although minor imperfections from manufacturing and residual thermal strains could result in different post-buckling responses.

So far, the test campaigns found in the literature on the fatigue study of the post-buckling response of stiffened composite panels only consider one combination of load level and load ratio, providing limited data to fully understand the phenomena governing the response of these structures during cyclic loads. To address this, the main objective of this study sought further understanding the behavior of stiffened composite panels with an initial delamination when subjected to fatigue in the post-buckling regime at different load levels and load ratios. Ten components consisting of a flat skin with a hat-stringer were manufactured and tested. Despite their small size, the specimens display a relative high level of complexity that allows to study the damage progression and failure in the post-buckling regime, while also providing data to verify quasi-static and fatigue numerical models. Two specimens were tested quasi-statically and eight were subjected to cyclic loads, considering four different fatigue scenarios by varying the maximum load and the load ratio to assess the effect of these parameters on the life of the components.

2. Specimen description

The single-stringer specimens investigated in this study are shown in Fig. 1 and consist of a flat skin co-cured with a hat-stringer. The skin is 320 mm long and 220 mm wide. The stringer, located in the center of the skin is 320 mm in length, 109 mm in width, and has a hat height of 32 mm. An initial delamination of 40 mm is artificially created by inserting a Teflon film between the skin and one of the stringer flanges. The components are made of IM7/8552 carbon-epoxy tape with a nominal ply thickness of 0.125 mm. The skin has eight plies with the quasi-isotropic lay-up $[45/90/-45/0]_S$, and the stringer is made of seven plies with the lay-up [−45/0/45/0/45/0/-45].

Some of the key steps of the manufacturing of the specimens are presented in Fig. 2. The manufacturing started with the manual cutting of the 15 plies of the skin and the stringer. The first skin ply was laid over the plate, vacuum sealed, and compacted by applying 3 min of full vacuum (Fig. 2a). This process was repeated every time a ply was laid until the skin lay-up was completed. Before continuing with the stringer lay-up, the stringer mold needed to be assembled. This mold is composed of three aluminum parts with a trapezoidal cross-section, 400 mm in length, and a tapered cross-section along the length to ease the disassembly and extraction of the mold after manufacturing (Fig. 2b).

Then, the Teflon insert and the stringer mold were placed over the skin, and the lay-up of the stringer was built following the same approach of the skin (Fig. 2c). To prepare the specimen for the autoclave, the debulking foil was removed and a thin fluorinated ethylene propylene release foil, the peel ply, and a breather blanket were placed over the specimen. The last preparation steps before the curing involved bagging the lay-up with seal tape and vacuum foil, sealing the bag, and checking for air leaks.

Once the sealed specimen was introduced into the autoclave (Fig. 2d), the autoclave was pressurized at 8 bar of absolute pressure and a vacuum of 200 mbar was enforced. The temperature of 110 °C was reached and maintained for 1 h. Then, the specimen was heated to 180 °C and maintained for another 2 h.

After the autoclave cycle, the stringer mold was disassembled and the specimens were cut to a length of 320 mm and a width of 220 mm with a circular saw using a diamond blade. Then, both short ends of the specimen were encased in 30 mm tabs made of metal-filled casting resin (Fig. 2e). As a consequence of casting, the free length of the specimens was reduced from 320 mm to 260 mm. The outermost faces from the tabs were machined after curing to ensure parallelism between them and perpendicularity with the stiffener center-line so that the compressive load could be applied uniformly.

To allow the use of Digital Image Correlation (DIC) measurements during the tests, the specimens were painted with white color and then with black speckles of approximately 1.5 mm in diameter providing around 40% of coverage over the white base. The center of mass was determined for the cross-section disregarding the resin tabs, so to be able to align the center of mass with the center of the loading plates to avoid any non-axial loads (Fig. 2f). The average and standard deviation values of the measurements, taken before the specimens were encased in the tabs, are reported in Table 1, and show a good consistency and low standard deviation.

3. Test set-up and sequence

The set-up used for the quasi-static and fatigue tests of the specimens is shown in Fig. 3. The tests were performed using a servo-hydraulic MTS 810 testing machine, equipped with a displacement sensor and a 500 kN load cell. Two linear variable displacement transducers (LVDTs) with a range of 10 mm were attached to the upper fixed plate of the test equipment and measure the vertical upwards displacement of the lower resin tabs of the specimens. The LVDTs were positioned on opposite sides of the specimens to quantify the end-shortening as well as to detect any possible load misalignment during the tests.

DIC systems VIC-3D 8 were used to measure the in-plane and out-of-plane displacements and the strains. They allowed to monitor the buckling and post-buckling shapes of the specimens during the propagation of the delamination. For all the tests, one three dimensional DIC system was used pointing at the specimen from the skin side, as seen in Fig. 3. Another system was added to measure the deformation from the

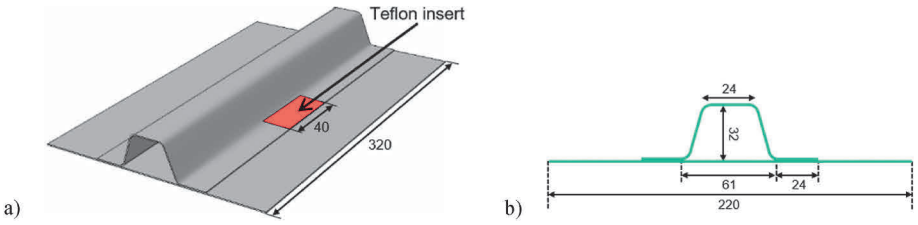

Fig. 1. Single-stringer composite specimen: a) isometric view; b) cross-section. (All dimensions in millimeters)

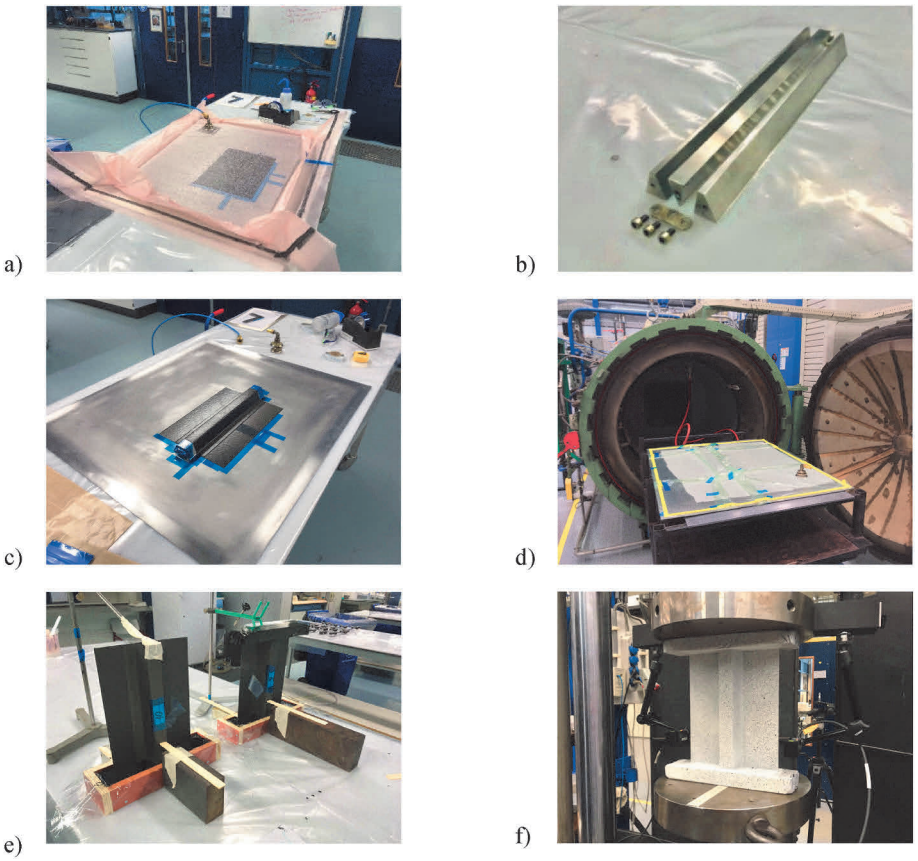

Fig. 2. Manufacturing process: a) debulking of skin plies; b) disassembled stringer mold; c) lay-up of stringer; d) specimen going into autoclave; e) casting of resin tabs; f) specimen ready for testing.

Table 1
Dimensions of single-stringer specimens (average value and standard deviation for the 10 specimens manufactured).

Length [mm]	Width [mm]	Skin thickness [mm]	Stringer thickness [mm]	Weight [g]
320.5 ± 1.3	220.7 ± 0.5	1.13 ± 0.01	0.90 ± 0.01	181.0 ± 2.5

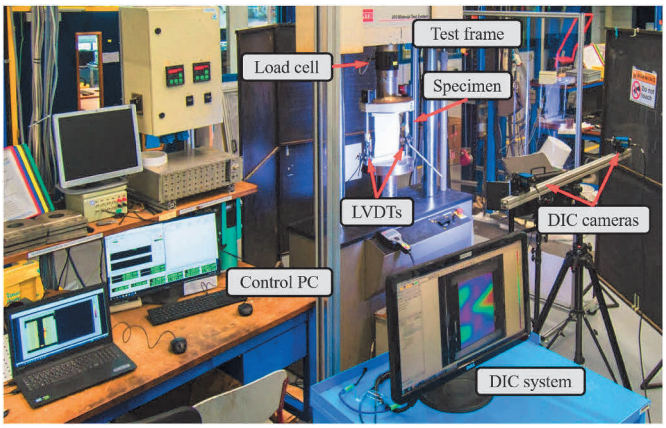

Fig. 3. Test set-up.

stringer side during the quasi-static tests. For the quasi-static tests, images were captured every 5 s; while, during fatigue, the images were taken every 250 cycles at the minimum and maximum load to monitor the out-of-plane displacement, allowing the early detection of the onset and propagation of the delamination. Moreover, a digital single-lens reflex (DSLR) camera was used to record video and take images of the specimens during and after the tests. One PC was needed to control the testing machine and manage data acquisition, and another PC was used to record the DIC data.

An ultrasonic through-transmission C-scan system, shown in Fig. 4, was used to track the progression of the delamination. To do so, specimens had to be removed from the testing machine and placed in a water tank where they were scanned with an Olympus OmniScan SX. The system consists of a 5 MHz ultrasonic signal emitter and a receiver, and, by placing the component between them, the signal damped by the

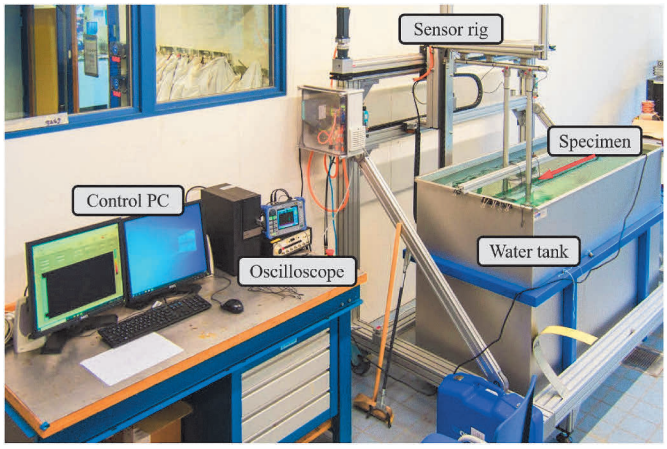

Fig. 4. Ultrasonic C-scan system.

specimen was measured with a resolution of 1 mm in both the horizontal and vertical axes. An initial C-scan was conducted for each specimen prior to testing to check for any manufacturing defects. Using this C-scan as a reference, the delamination front could be tracked by observing a decrease in the signal reaching the receiver as a consequence of the damping and diffraction caused by the delamination. C-scans were performed during quasi-static tests, and every 1000 cycles for the fatigue tests. The data obtained from the ultrasonic inspections were used to assess when the initial damage started to increase in size, referred to as the delamination onset, and to measure the growth of the delamination length.

A typical image obtained from the C-scan is shown in Fig. 5. The part of the specimen without damages corresponds to the green color, while damage is reported in yellow, red, or black depending on how much signal is damped and diffracted. No information regarding the position of the damage through the thickness can be retrieved from the used C-scan system. The delamination length reported for the specimens was calculated manually by averaging three measurements of the delaminated length along the centerline of the stringer foot over the initial delamination, and at the inner and outer edges of the stringer foot. In Fig. 5 it can also be seen how the central part of the specimen features a vertical thick black stripe due to the air trapped within the hat-stringer, which does not transmit the signal as water does. Two thin red vertical lines can also be noted. They are caused by the diffraction of the signal by the stringer feet bevels as their surface is not perpendicular to the direction of signal emission. An average delamination length was taken to determine the propagation of the damage during the tests.

The test campaign consisted of two quasi-static tests of specimens, named SSCS1 and SSCS2, and eight fatigue tests of specimens, named SSCS3 to SSCS10. Specimens SSCS1 and SSCS2 were subjected to quasi-static compressive loads under displacement-controlled conditions with a loading rate of 0.1 mm/min until the collapse. Four different load scenarios were considered for the fatigue tests, changing both the maximum load and the load ratio. Fatigue testing was always conducted under load-controlled conditions at a frequency of 2 Hz. Three different values for the maximum load were selected based on the quasi-static test results: 25.2 kN, 27.1 kN, and 29.2 kN.

These load levels correspond to 90%, 95%, and 105% of the average delamination onset loads of specimens SSCS1 and SSCS2; that is also equal to about 75%, 80%, and 85% of their average collapse load, and approximately 200%, 215%, and 230% their average collapse load.

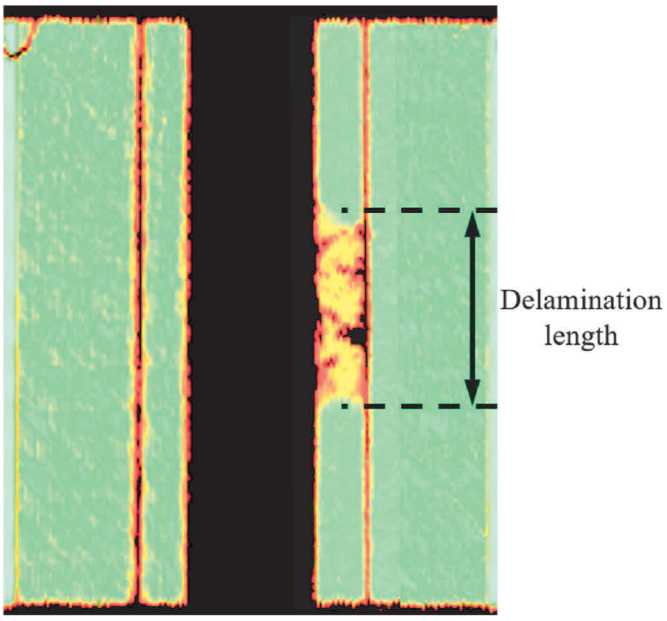

Fig. 5. C-scan and delamination length.

Moreover, to assess the influence of the load ratio, the fatigue tests at 29.2 kN were performed with two load ratios, R = 0.1 and R = 0.5. Two specimens were tested for each load scenario. A summary of the tests is reported in Table 2.

4. Quasi-static tests of SSCS1 and SSCS2

Quasi-static tests were conducted on two specimens, SSCS1 and SSCS2. Each test was stopped a few times, unloading the specimens and removing them from the test equipment. This was done to perform an ultrasonic C-scan and evaluate the delamination propagation. Then, the specimens were carefully repositioned into the test equipment and loaded again. In particular, the quasi-static test of SSCS1 was stopped eight times, progressively increasing the maximum displacement until the specimen collapse, while the test of SSCS2 was stopped three times. The curves obtained from each loading of SSCS1 and SSCS2 are presented in Fig. 6a and b, respectively, reporting as well the combined curve represented by the thick solid line in the graphs. These combined responses for SSCS1 and SSCS2 are presented as standalone curves in Fig. 7, where it can be seen that the response of both specimens is almost identical until the load of 25 kN, with only a minor difference in the stiffness values during the pre- and post-buckling fields.

In order to explain the post-buckling behavior and the collapse, Fig. 8 reports the evolution of the out-of-plane displacements of SSCS2 measured using the DIC from the stringer and skin sides, and the C-scans, at four different loads. The out-of-plane displacements are reported in millimeters, and positive values indicate displacements towards the viewer.

The buckling shape of SSCS2 at 15 kN is shown in Fig. 8a, and presents two half-waves on each side of the skin with a maximum out-of-plane displacement of 2.6 mm. It can be seen that one half-wave was also forming in the central part of the component below the stringer. The C-scan shows that the initial delamination of the Teflon insert is still intact.

The delamination onset is identified with the propagation of the initial delamination of the 40 mm Teflon insert. This occurred at 26.5 kN for SSCS2, and was identified by a loud noise and a sudden load drop of approximately 3.0 kN. Fig. 8b shows the specimen after the delamination onset, and a significant buckling shape change can be identified in the form of one half-wave on the delamination side propagating below the stringer, and three half-waves on the opposite side. The maximum out-of-plane displacement was 5.8 mm. The C-scan shows an increase of the delamination length from the initial 40 mm–76 mm.

When loading was resumed after the delamination onset, the stiffness of the specimen reduced from approximately 47 kN/mm to 31 kN/mm. The load continued to increase until the delamination propagated to the stiffener foot opposite to the initial delamination. This event occurred at 30.9 kN for SSCS2, and was identified from a soft noise and a small load drop of approximately 0.1 kN. From Fig. 8c, it is possible to note that the maximum out-of-plane displacement of SSCS2 had grown to 7.7 mm and five small half-waves appeared on the top of the stringer. The C-scan shows that the delamination increased from 76 to 79 mm, and also

Table 2
Specimen name and type of performed tests.

Specimen	Test type	Fatigue load [kN]	Load ratio
SSCS1	Quasi-static	–	–
SSCS2	Quasi-static	–	–
SSCS3	Fatigue	25.2–2.52	0.1
SSCS4	Fatigue	25.2–2.52	0.1
SSCS5	Fatigue	27.1–2.71	0.1
SSCS6	Fatigue	27.1–2.71	0.1
SSCS7	Fatigue	29.2–2.92	0.1
SSCS8	Fatigue	29.2–2.92	0.1
SSCS9	Fatigue	29.2–14.6	0.5
SSCS10	Fatigue	29.2–14.6	0.5

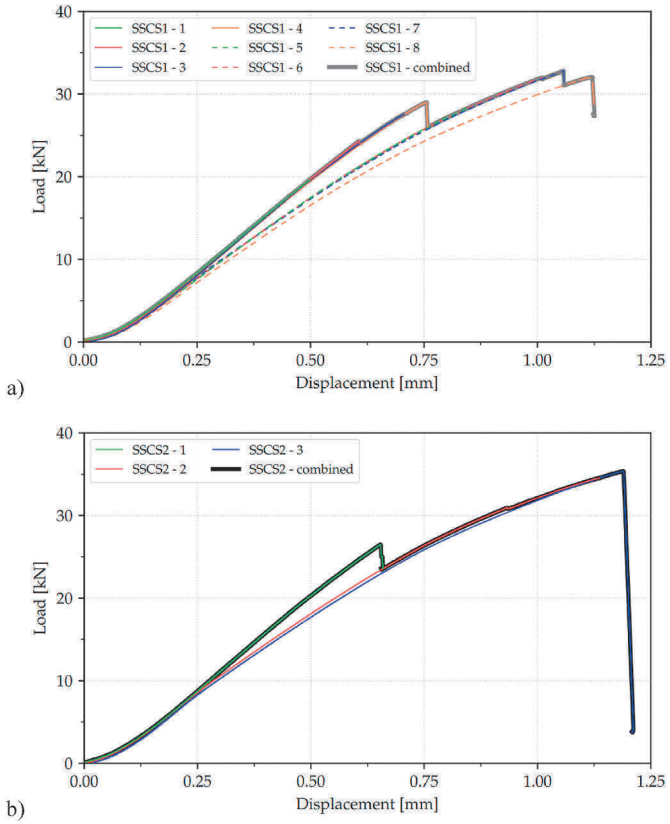

Fig. 6. Load-displacement curves of quasi-static loading and combined curve: a) SSCS1; b) SSCS2.

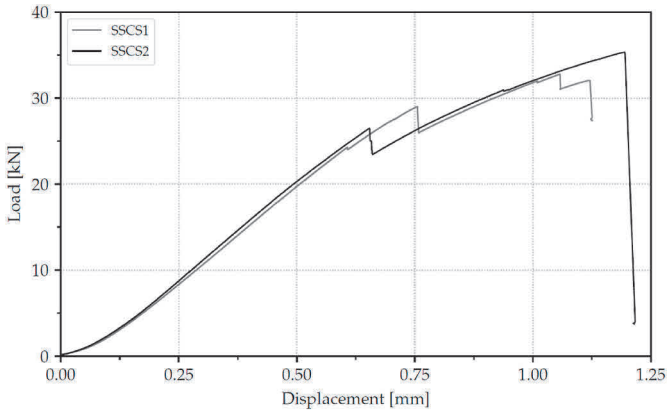

Fig. 7. Load-displacement curves of quasi-static tests of SSCS1 and SSCS2.

resulted in a separation with a half-moon shape on the opposite stringer foot (circled in red in the C-scan image of Fig. 8c).

After the delamination propagation to the opposite stringer foot, the stiffness of the specimen further reduced to approximately 16 kN/mm. When the compressive load reached 35.4 kN, the collapse of the specimen occurred. This event was marked by an abrupt load drop caused by the separation of the skin from the central area of the stringer feet and the stringer crippling. In the images of SSCS2 after the collapse (Fig. 8d), it can be seen that the delamination had propagated so to cause the complete separation of the skin from the stringer, creating a tunnel under the stringer and a consequent stringer crippling. The C-scan of the post-mortem specimen revealed a delamination length of 112 mm on the Teflon side.

Specimen SSCS1 had a similar structural behavior. Fig. 9 reports the out-of-plane displacements of SSCS1 measured by DIC from the skin side at the same four states presented in Fig. 8 for SSCS2. The buckling shape of SSCS1 at 15 kN is reported in Fig. 9a. It presents three half-waves on each skin side, slightly differing from the buckling shape of SSCS2. The delamination onset of SSCS1 occurred at 29.5 kN with a load drop also around 3.0 kN. Fig. 9b shows the corresponding out-of-plane displacement, which resembled the buckling shape of SSCS2 after the delamination onset. The delamination propagated to the stringer foot opposite to the initial Teflon insert at 32.5 kN, a load slightly higher than for SSCS2 (Fig. 9c). The specimen collapsed at 33.3 kN also in this case with the formation of a tunnel between the skin and the stiffener and a consequent stringer crippling (Fig. 9d).

A comparison of the loads at delamination onset, at propagation of the delamination to the opposite stringer foot and at collapse for specimens SSCS1 and SSCS2, and their average, is reported in Table 3. The values show that the specimens can withstand loads nearly 20% higher than the delamination onset load before collapse occurs.

The measurement of the DIC allowed to retrieve also the strain distributions. The strains of the outermost skin ply of SSCS2 are shown in Fig. 10, at the delamination onset, at the propagation of the delamination to the opposite stringer foot, and at the collapse. In correspondence of the delamination onset, the maximum compressive strains along the specimen axis (ε_{yy}) reached approximately 5200 $\mu\varepsilon$ over the location of the initial delamination, indicated with the purple region in Fig. 10a. Approximately the same value was also measured during the test of SSCS1.

At the propagation of the delamination to the opposite stringer foot, the maximum tensile strains along the x-axis (ε_{xx}) reached 2690 $\mu\varepsilon$ on the central part of the skin, indicated with the red region in Fig. 10b. At the final collapse, the maximum tensile strain values along the y-axis was around 5800 $\mu\varepsilon$ measured on the large half-wave over the initial delamination, and indicated with the red area of Fig. 10c.

The post-mortem photos of specimens SSCS1 and SSCS2 are presented in Fig. 11. The stringer crippling can be identified in the central part of the stiffeners for both specimens. In SSCS2 fiber pull-out can be also observed, following the 45° direction of the outermost skin ply.

5. Fatigue tests of SSCS3 – SSCS6: maximum loads 25.2 kN and 27.1 kN, load ratio R = 0.1

Specimens SSCS3 – SSCS6 were tested in fatigue with a load ratio of 0.1 and two different maximum loads: 25.2 kN for specimens SSCS3 and SSCS4, and 27.1 kN for SSCS5 and SSCS6. Before applying the first fatigue cycle, an initial quasi-static test was performed until the maximum fatigue load to check the stiffness of the specimens. Then, the fatigue cycling was started. The evolution of the out-of-plane displacements and the C-scans measured on SSCS4 are presented in Fig. 12. Fig. 12a shows the out-of-plane displacements and the C-scan on the first cycle at 25.2 kN. The buckling shape had two half-waves on the skin side with the Teflon insert and three half-waves on the opposite side, with a maximum out-of-plane displacement of 3.2 mm. From the C-scan it can be seen that the initial delamination had not yet propagated.

The delamination onset of SSCS4 occurred at 18500 cycles (Fig. 12b), and was detected by a sudden noise and the change in the buckling shape. The two half-waves on the side with the Teflon insert turned into a large half-wave with a maximum out-of-plane displacement of 6.5 mm. This buckling shape was similar to the one seen after the delamination onset during the quasi-static tests of SSCS1 and SSCS2. The C-scan revealed that the delamination length of SSCS4 had grown to 73 mm. The maximum out-of-plane displacement and the delamination size increased with the increase of the number of cycles, measuring 6.9 mm and 85 mm, respectively at 50000 cycles (Fig. 12c). As fatigue testing continued the buckling shape did not change, although the delamination size and the maximum out-of-plane displacement continued to increase. At 150000 cycles (Fig. 12d) the maximum out-of-plane displacement measured 7.1 mm, and the delamination length 98

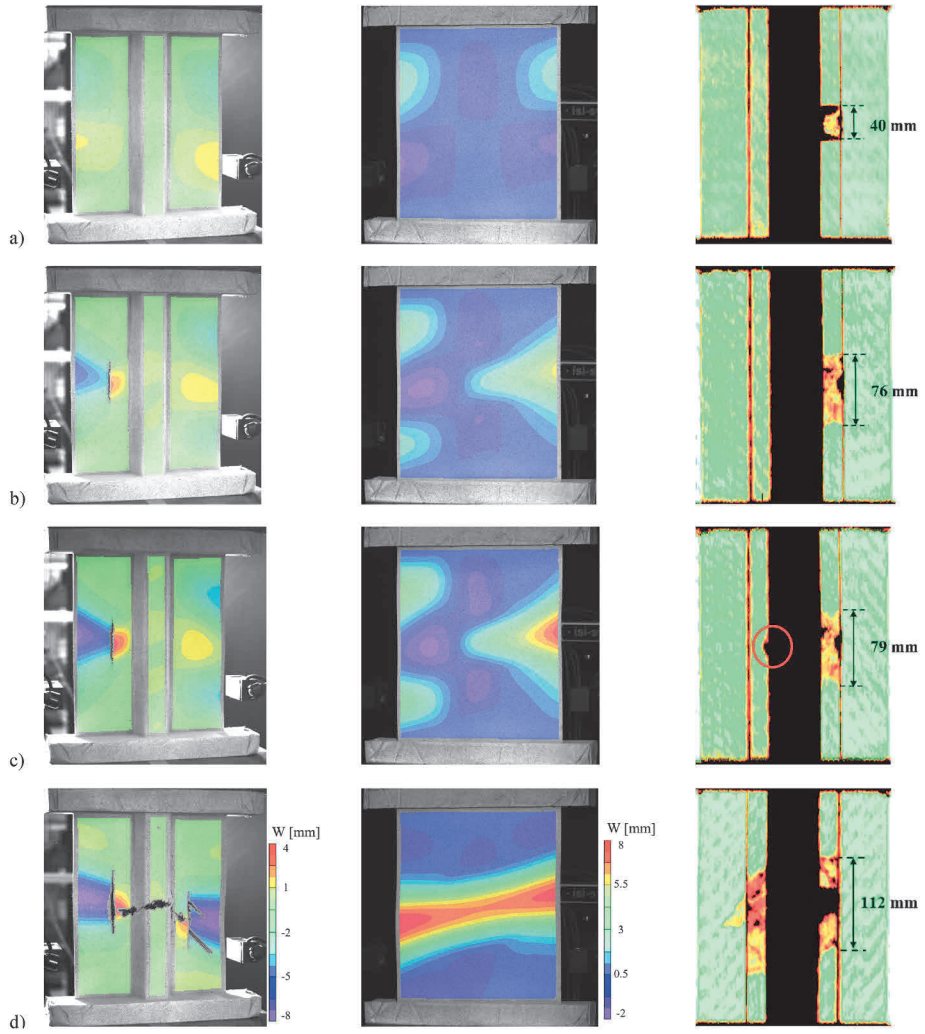

Fig. 8. Quasi-static test of SSCS2. DIC from stringer side, DIC from skin side, C-scan: a) 15.0 kN; b) 23.6 kN; c) 30.9 kN; d) after collapse.

mm.

The behavior of the four specimens SSCS3 – SSCS6 during fatigue cycling was similar. All four specimens reached 150000 cycles without collapse. However, as a consequence of testing at different load levels the delamination onset occurred at a lower number of cycles for SSCS5 and SSCS6. The delamination onset of SSCS3 and SSCS4 happened at 6725 and 18500 cycles respectively, whereas it occurred during the first cycle for SSCS5 and at 2450 cycles for SSCS6.

The extension of the damaged area was monitored with regular ultrasonic inspections for all four specimens. The delamination length is plotted against the cycle count in Fig. 13. This graph shows a difference between SSCS3 and SSCS4 during the initial 75000 cycles, where SSCS3 was characterized by a smooth increment in delamination length after the delamination onset, while SSCS4 showed an abrupt increase of 33 mm in the delamination length at the onset. Then, between 25000 and 75000 cycles the rate of delamination growth for SSCS3 is slightly higher than that of SSCS4. During the last 75000 cycles the delamination length of both specimens increased approximately 10 mm following a similar growth rate.

In the case of specimens SSCS5 and SSCS6, the trends observed during the propagation of the delamination are more similar. For both specimens, the initial delamination grew from 40 mm to approximately 56 mm. Moreover, both curves run nearly parallel throughout most of the fatigue testing with the delamination length of specimen SSCS6 around 8–12 mm consistently shorter than that of SSCS5 for the same number of cycles.

All four specimens were able to sustain 150000 cycles. The curves of Fig. 13 show that the propagation of the delamination reached an almost plateau phase, with little growth in the last 50000 cycles and all delamination lengths converging towards 95–98 mm. Considering that this type of components of aeronautical structures are not expected to go so many cycles into the post-buckling regime, after reaching 150000 cycles, it was decided to subject the specimens to a quasi-static test until final collapse to evaluate the reduction of their load-bearing capacity due to fatigue.

The load-displacement responses from the quasi-static tests after the fatigue cycles are reported in Fig. 14, where the curve of the quasi-static test of SSCS2 is also added for comparison. The maximum load before collapse decreased from an average 34.4 kN for SSCS1 and SSCS2 to an average of 32.6 kN (−5.2%) for SSCS3 and SSCS4, and to 31.3 kN (−9.0%) for SSCS5 and SSCS6. Table 4 reports a summary of these tests, including data from fatigue and quasi-static tests until collapse.

The collapse seen during the quasi-static tests after fatigue had a similar behavior of the collapse of SSCS1 and SSCS2. Fig. 15 reports the images taken by the DLSR camera, the out-of-plane displacements measured on the skin side, and the C-scans of SSCS4 immediately before and after collapse. The DSLR images are mirrored with respect to the DIC images and the C-scans. Specimen SSCS4 was able to sustain up to 33.2 kN. At that load, the delamination front propagated to the opposite stringer foot (Fig. 15a), which resulted in a load drop to 32.5 kN and a sudden noise. With the C-scan it can be seen that the propagation of the delamination had formed a half-moon shape on the opposite stringer

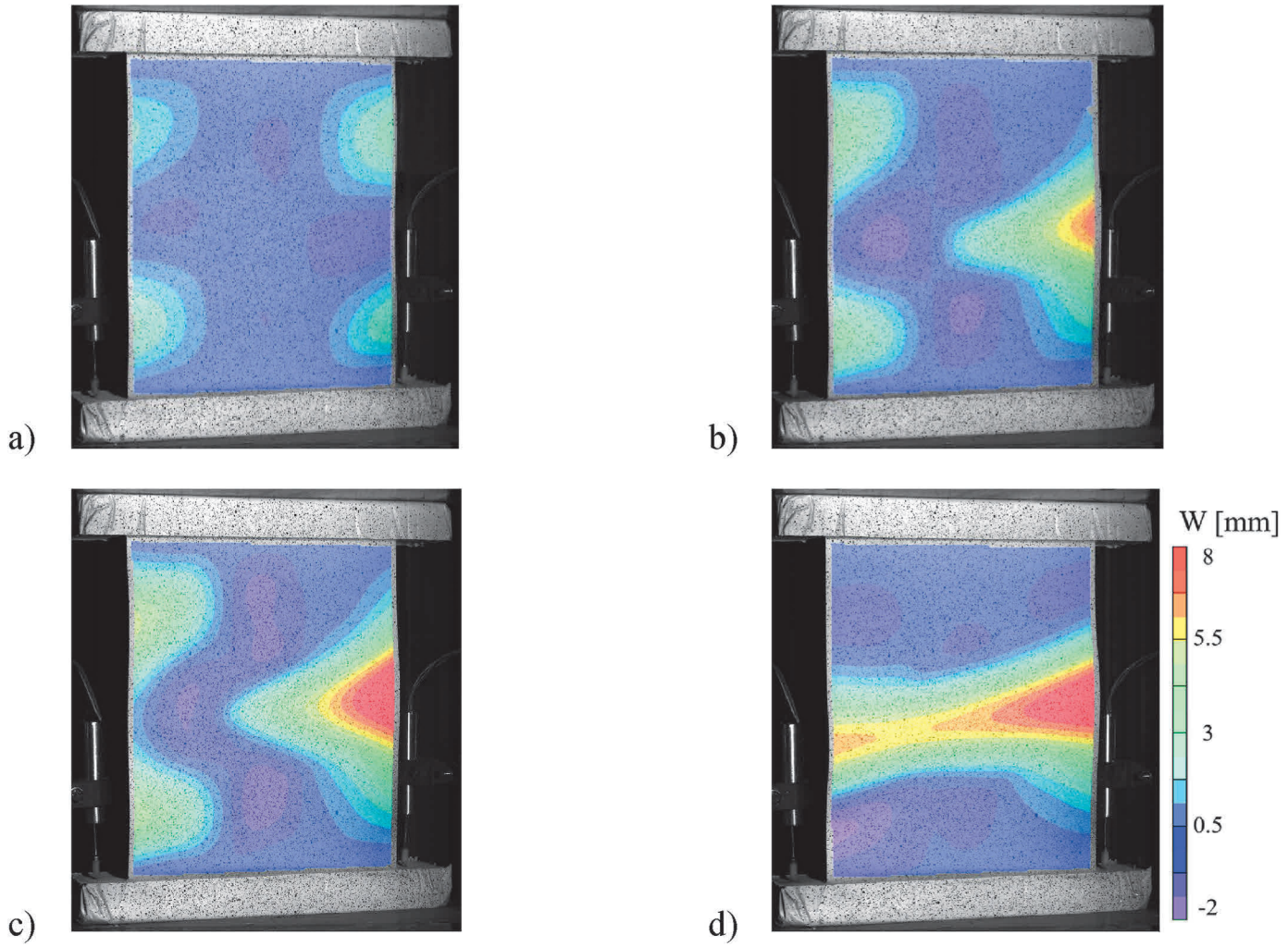

Fig. 9. Quasi-static test of SSCS1, DIC from skin side: a) 15 kN; b) 26.3 kN; c) 32.5 kN; d) after collapse.

Table 3
Summary of quasi-static tests of specimens SSCS1 and SSCS2.

Specimen	Load at delamination onset [kN]	Load at propagation to opposite stringer foot [kN]	Collapse load [kN]
SSCS1	29.5	32.5	33.3
SSCS2	26.5	30.9	35.4
Average	28.0	31.7	34.4

foot as it had occurred in the tests of SSCS1 and SSCS2. The specimen was placed again under the testing machine and the quasi-static test was resumed. The specimen collapsed when the load reached 33.0 kN as the delamination fully propagated leading to the tunneling and stringer crippling (Fig. 15b).

Similarly, the images from the DLSR camera, the out-of-plane displacements measured on the skin side, and the C-scans of SSCS6 before and after the specimen collapsed are reported in Fig. 16. Specimen SSCS6 was able to sustain up to 29.7 kN. At that load, the stringer foot on the side of the Teflon insert failed, causing a load drop to 25.8 kN (Fig. 16a). The C-scan performed afterwards revealed that the delamination front had an approximate length of 96 mm and also extended to the opposite stringer foot forming the half-moon shape. Then, tunneling and stringer crippling occurred as shown in Fig. 16b, leading to the final collapse of the component.

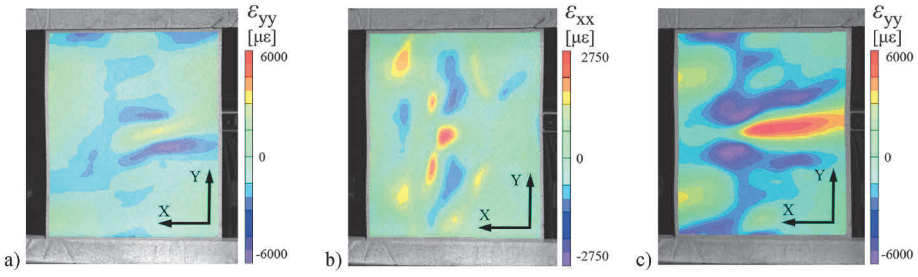

Fig. 10. Strains during quasi-static test of SSCS2: a) ε_{yy} at delamination onset (26.5 kN); b) ε_{xx} at propagation of the delamination to opposite stringer foot (30.9 kN); c) ε_{yy} at specimen collapse (35.4 kN).

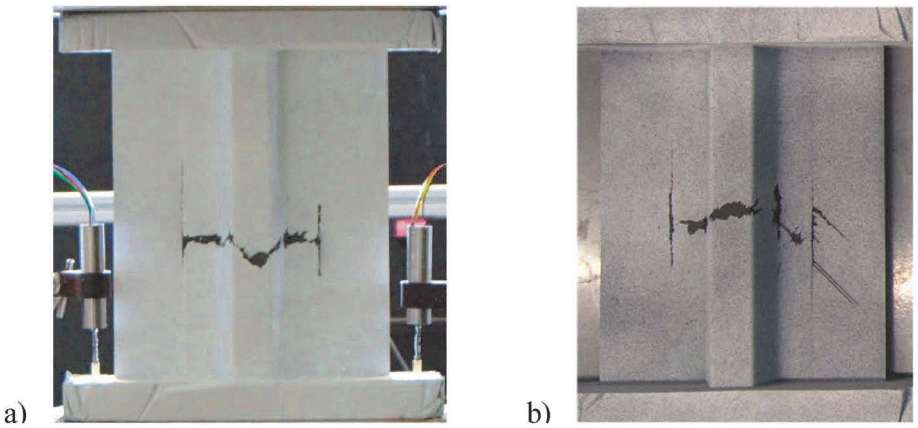

Fig. 11. Specimens after collapse: a) SSCS1; b) SSCS2.

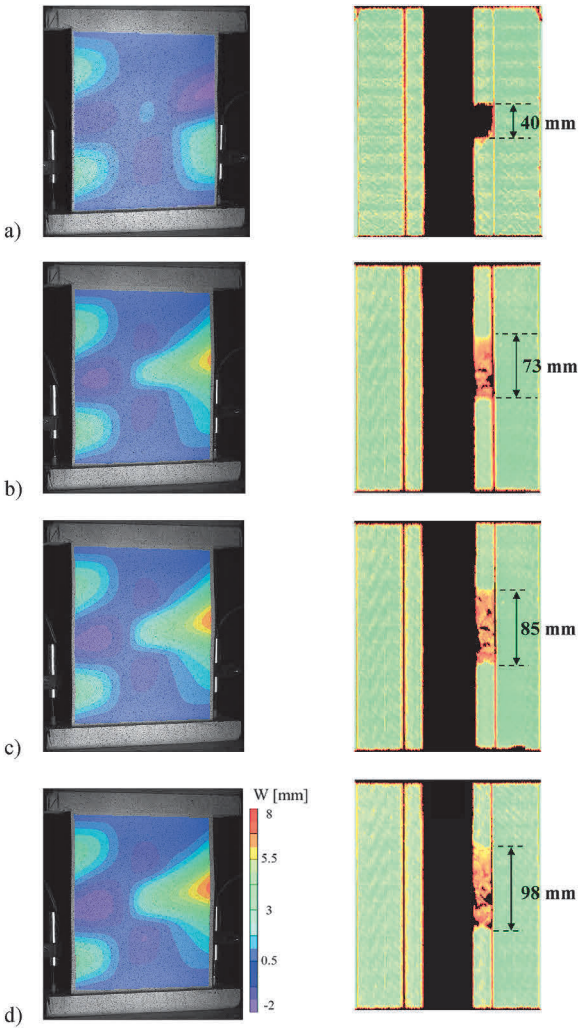

Fig. 12. Fatigue test of SSCS4, DIC from skin side and C-scan: a) first cycle; b) 18500 cycles; c) 50000 cycles; d) 150000 cycles.

Fig. 17 reports the post-mortem images of SSCS4 and SSCS6 after the collapse. It can be seen that the stringer crippling of SSCS4 followed a path at 90° with respect to the stringer axis (Fig. 17a), while the stringer crippling of SSCS6 followed the direction of 45° (Fig. 17b).

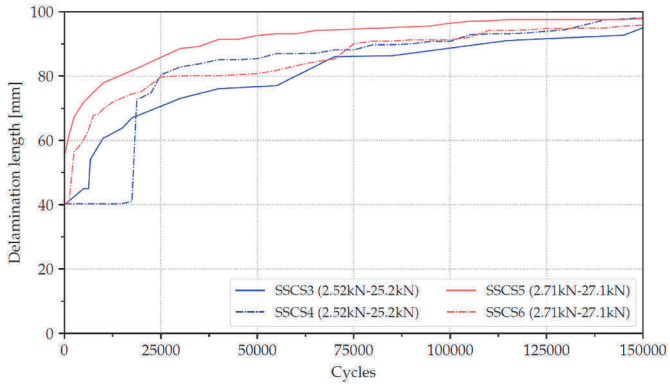

Fig. 13. Delamination length versus cycle count for specimens SSCS3 to SSCS6.

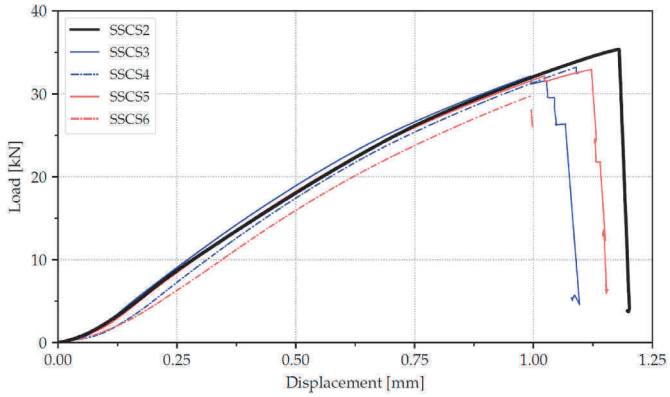

Fig. 14. Quasi-static tests of SSCS3 – SSCS6 after fatigue, and quasi-static test of SSCS2.

6. Fatigue tests of SSCS7 – SSCS10: maximum load 29.2 kN, load ratios R = 0.1 and R = 0.5

As there was no collapse during 150000 cycles for specimens SSCS3 – SSCS6, the maximum load of the fatigue tests for specimens SSCS7 – SSCS10 was increased to 29.2 kN. Two load ratios were chosen to investigate the effect of this parameter on the fatigue behavior: R = 0.1 for SSCS7 and SSCS8, and R = 0.5 for SSCS9 and SSCS10.

Fig. 18 reports the out-of-plane displacements measured by the DIC system taken from the skin side of SSCS8 and SSCS10 during the first cycle, while Fig. 19 reports the out-of-plane displacements at 10000 cycles, both at the maximum and minimum loads. It is possible to note

Table 4
Summary of fatigue tests and static collapse loads of specimens SSCS3 – SSCS6.

Specimen	Fatigue load [kN]	Total cycles	Delamination onset [cycles]	Delamination length after fatigue [mm]	Maximum load [kN]
SSCS3	25.2–2.52	150000	6725	95.1	32.1
SSCS4	25.2–2.52	150000	18500	98.1	33.2
SSCS5	27.1–2.71	150000	1	97.9	32.9
SSCS6	27.1–2.71	150000	2450	95.8	29.7

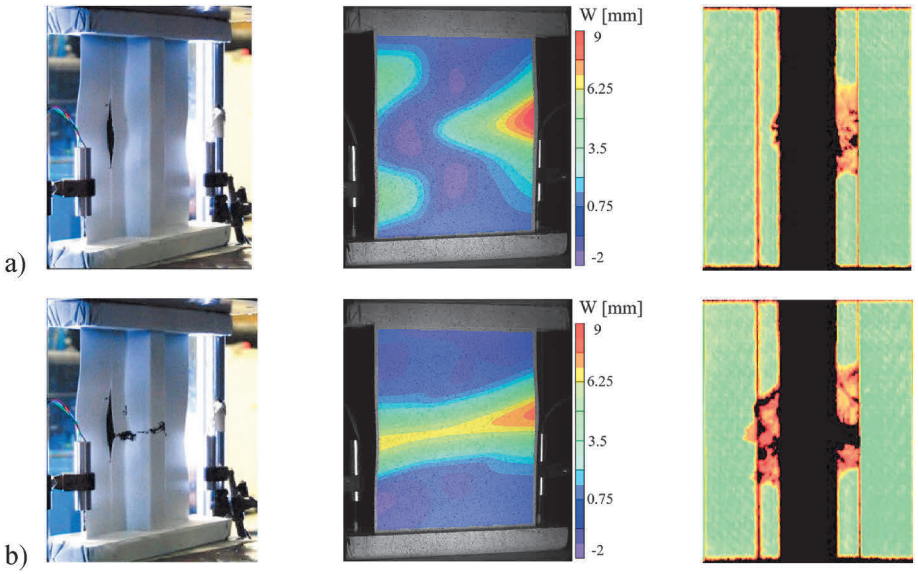

Fig. 15. Collapse sequence of SSCS4 during quasi-static test after fatigue. Images from camera, DIC from skin side, C-scans: a) 32.5 kN; b) after collapse.

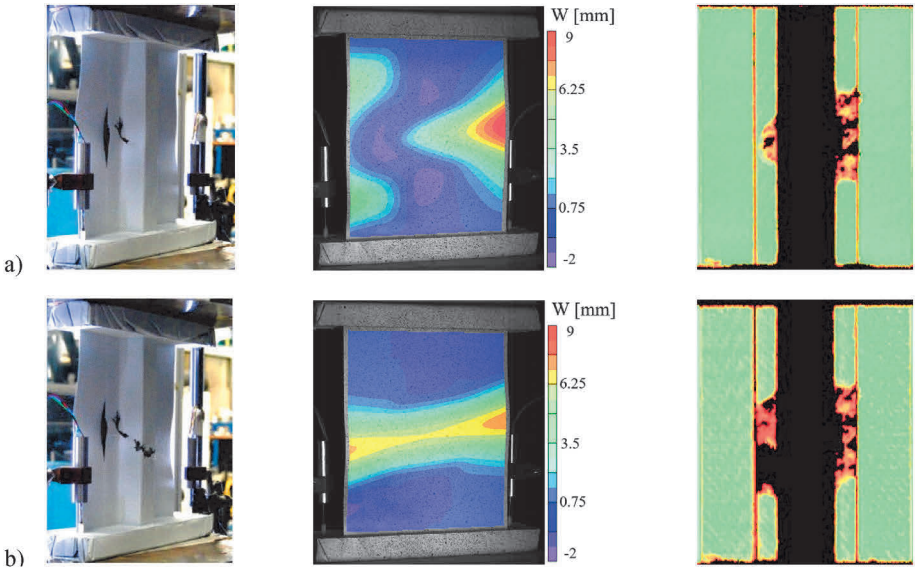

Fig. 16. Collapse sequence of SSCS6 during quasi-static test after fatigue. Images from camera, DIC from skin side, C-scans: a) 25.8 kN; b) after collapse.

that specimen SSCS8, tested with R = 0.1, cycled between the pre-buckled and post-buckled shape, while specimen SSCS10 was already buckled at its minimum fatigue load of 14.6 kN, thus cycled in the post-buckling regime.

The evolution of the out-of-place displacements of SSCS8 at maximum load at four different cycles is reported in Fig. 20, together with the corresponding C-scans. Fig. 20a shows the out-of-plane displacements and the C-scan at the first fatigue cycle. The maximum out-of-plane displacement is equal to 4.5 mm, and the C-scan shows that the initial delamination had not yet grown in size.

The delamination onset occurred at 550 cycles (Fig. 20b), accompanied by a change in buckling shape, and the delamination length growth from 40 to 66 mm. The buckling shape at 10000 cycles is reported in Fig. 20c. The maximum out-of-plane displacement reached 8.3 mm, and the C-scan revealed that the delamination length was 82 mm and had propagated on the opposite stringer foot.

The out-of-plane displacements at 13000 cycles are shown in Fig. 20d. The overall buckling shape of the specimen did not change

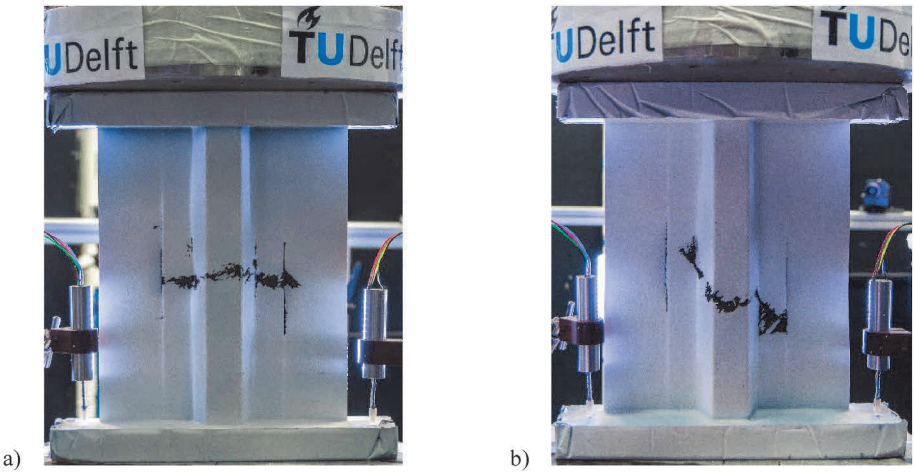

Fig. 17. Specimens after collapse: a) SSCS4; b) SSCS6.

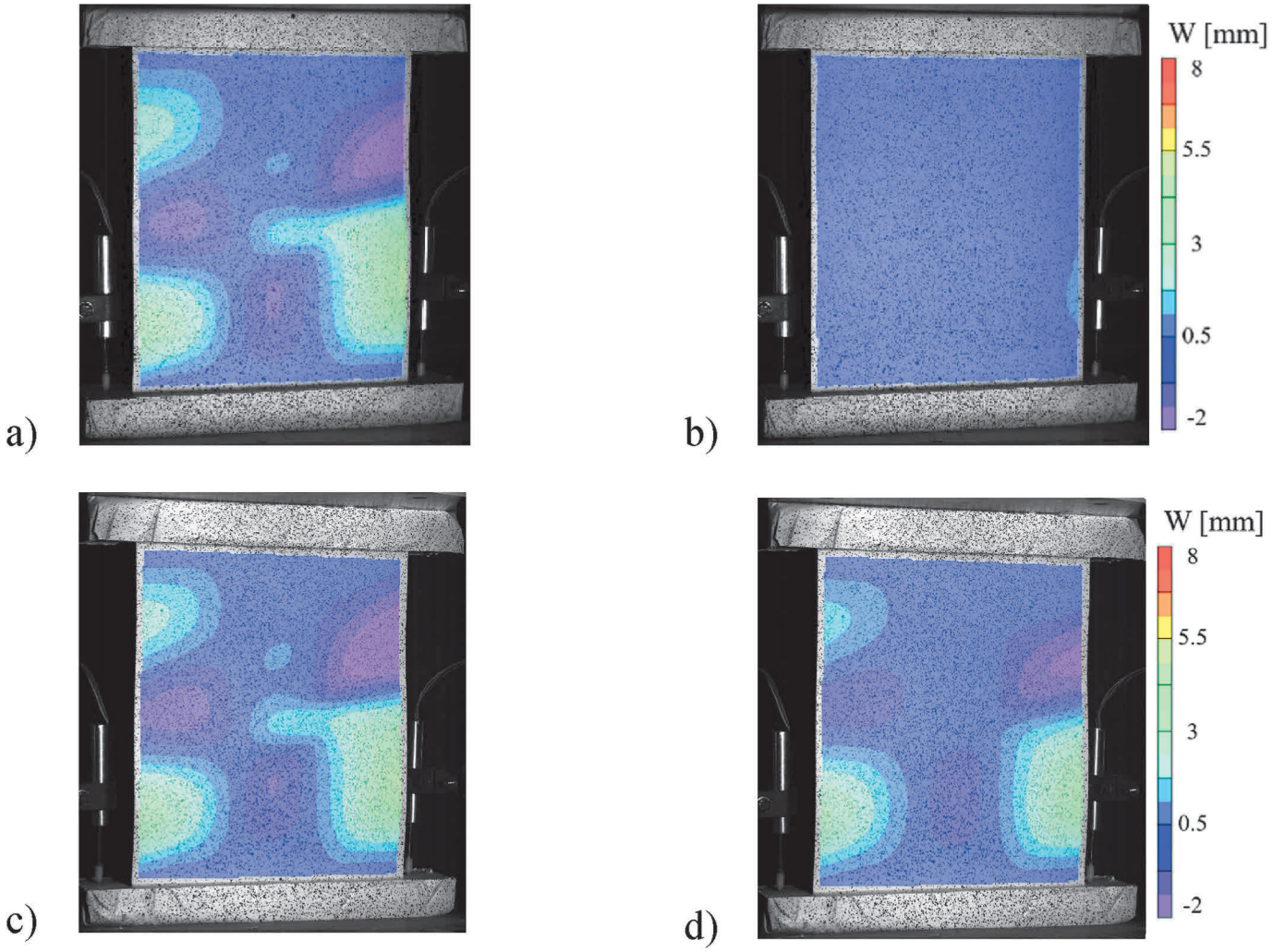

Fig. 18. DIC from skin side of SSCS8 and SSCS10 at first cycle: a) SSCS8 at 29.2 kN; b) SSCS8 at 2.92 kN; c) SSCS10 at 29.2 kN; d) SSCS10 at 14.6 kN.

significantly, although there was an increase in the maximum out-of-plane displacement, with a maximum value of 8.6 mm. From the C-scan a delamination length of 87 mm was measured. When fatigue testing resumed, specimen SSCS8 withstood another 446 cycles before the collapse.

The evolution of the out-of-plane displacements of specimen SSCS10 was similar to that of SSCS8. The delamination onset occurred at 70 cycles, but then the delamination grew slower. To illustrate the effect of the load ratio on the growth rate of the delamination length, a comparison between the C-scans of SSCS8 and SSCS10 at different cycles is

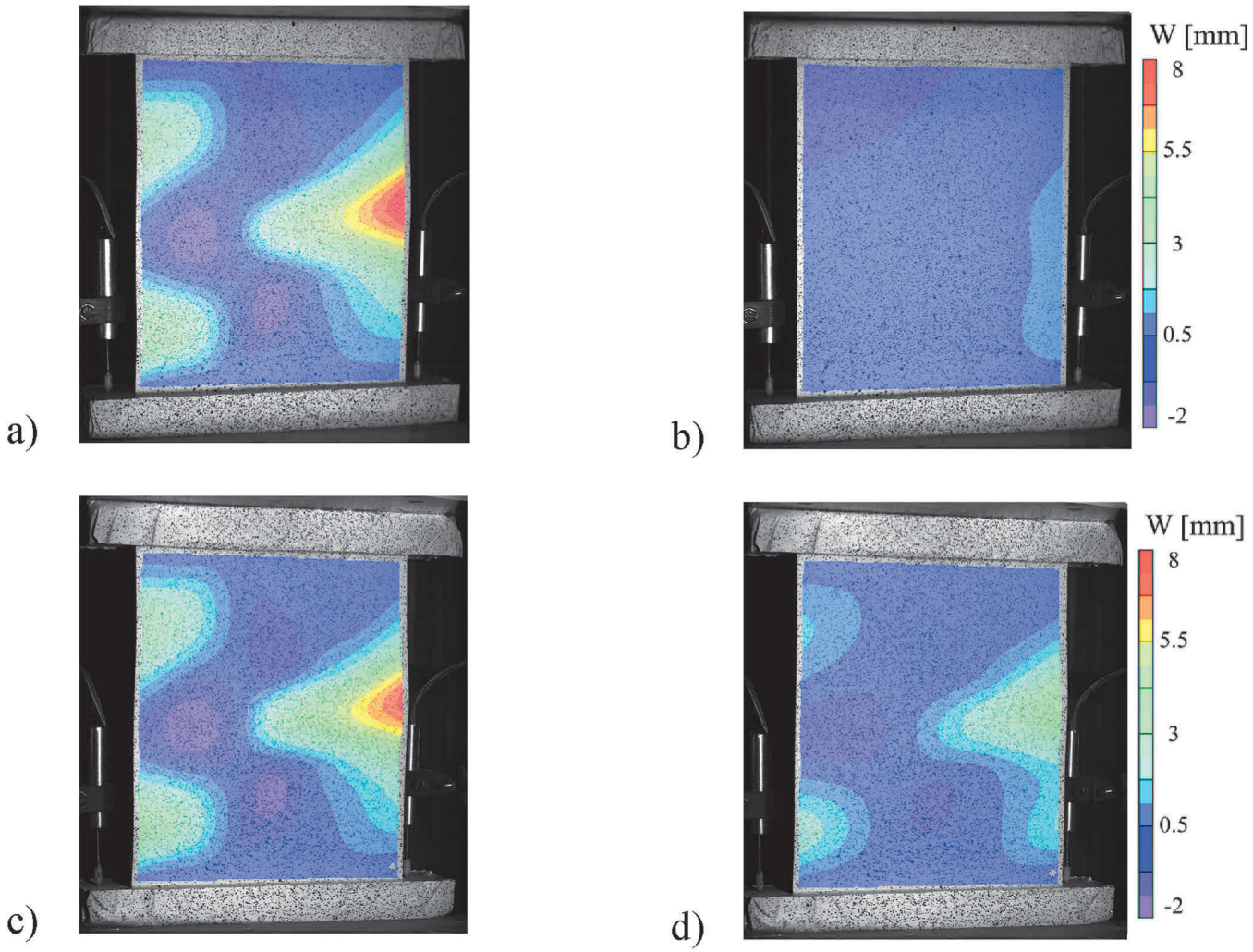

Fig. 19. DIC from skin side of SSCS8 and SSCS10 at 10000 cycles: a) SSCS8 at 29.2 kN; b) SSCS8 at 2.92 kN; c) SSCS10 at 29.2 kN; d) SSCS10 at 14.6 kN.

reported in Fig. 21. The first row of images (Fig. 21a) corresponds to the C-scans of SSCS8 and the second row (Fig. 21b) to those of SSCS10. The C-scans in the same column are at the same number of cycles: first cycle, 8000, 10000, 12000, and 16000 cycles, respectively. When the specimens reached 8000 cycles, the delamination of SSCS8 was 4 mm longer than that of SSCS10. At 10000 cycles, the difference in delamination length between the two specimens increased to 5 mm. At 12000 cycles, the extension of the damage was larger for SSCS8, with 6 mm difference. The collapse of SSCS8 happened at 13446 cycles. The last C-scan performed before the collapse of SSCS10 was performed at 16000 cycles, where a total delamination length of 80 mm was measured. For both specimens, the last C-scan before the collapse showed that the delamination had propagated to the opposite stringer foot with the half-moon shape.

The measurement of the delamination length every 1000 cycles yielded the graph shown in Fig. 22, where the data of specimens SSCS7 – SSCS10 are reported and the collapses are marked with a cross. As seen, the collapse sequence was due to the delamination that propagated to the opposite stringer foot, followed by the stringer crippling that caused the collapse. It can be noted that the growth rate and delamination size of all the specimens is closely matched during the initial 7000 cycles. Then, the effect of the different load ratio becomes evident, as the specimens tested with R = 0.1 exhibited a faster propagation of the delamination length than those tested with R = 0.5. The fatigue with a lower load ratio also led to earlier collapse and larger delamination lengths. Collapse happened at an average of over 10900 cycles and a delamination of 83.7 mm for the specimens tested with R = 0.1, whereas specimens tested with R = 0.5 collapsed at approximately 14530 cycles (33% more cycles than with R = 0.1) with a delamination length of 80.4 mm. Table 5 reports a summary of the tests results of specimens SSCS7-SSCS10.

7. Summary and discussion of the results

The results obtained from the test campaign here presented offered information in terms of buckling behavior, damage propagation, and collapse sequence of hat-stiffened composite panels. Moreover, since the tests were performed under quasi-static loading and four different fatigue scenarios, the effect of load levels and load ratios on the overall response could also be assessed.

The buckling behavior of the specimens does not vary significantly between quasi-static and fatigue loads. There are slight disparities before the delamination onset in terms of the number of half-waves formed on the skin, but these differences in the buckling shape can be attributed to small initial geometrical imperfections.

The delamination onset occurs at loads nearly twice the buckling load of the specimens. After the delamination onset, the buckling shape of the skin for all specimens developed one half-wave on the Teflon side and three half-waves on the opposite skin side. As the delamination fronts propagate, the large half-wave increases in extension and in out-of-plane displacement, until the delamination begins to propagate to the opposite stringer foot with a half-moon shape. This event occurred

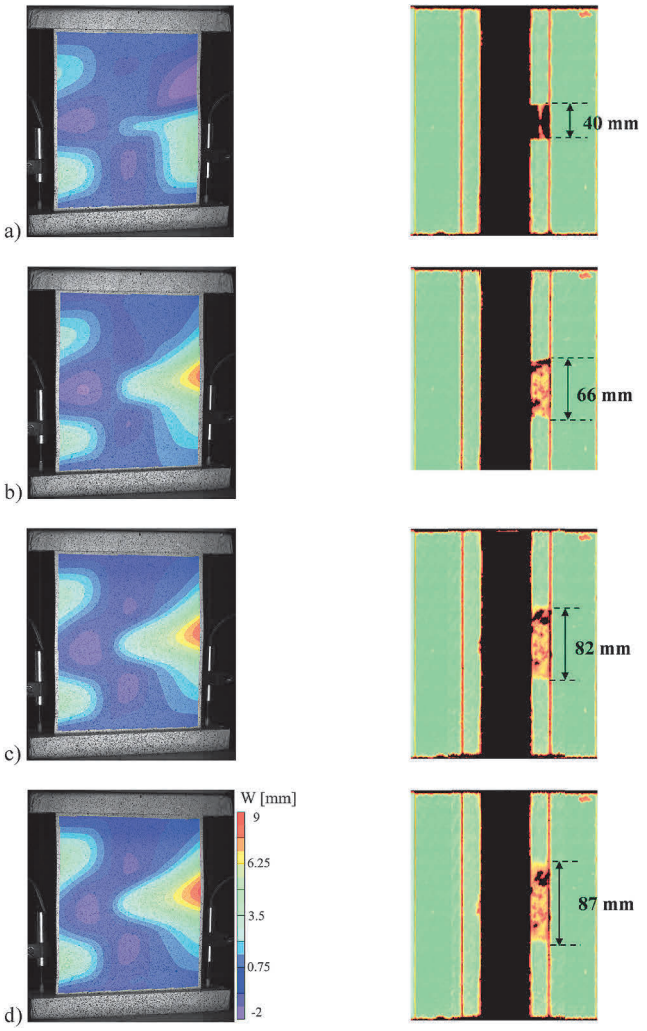

Fig. 20. Fatigue test of SSCS8, DIC from skin side and C-scan: a) first cycle; b) 550 cycles; c) 10000 cycles; d) 13000 cycles.

between 30.9 and 32.5 kN for the quasi-static tests of SSCS1 and SSCS2. In the case of the fatigue tests of specimens SSCS3 – SSCS6 this propagation did not occur during the 150000 cycles, but rather during the quasi-static test performed after, at loads between 29.7 and 32.5 kN. For specimens SSCS7 – SSCS10 the propagation of the damage to the opposite stringer foot took place during fatigue testing at approximately 8000 cycles for a load ratio 0.1 and at approximately 12000 cycles for the load ratio 0.5.

The data measured on all fatigue tests are reported in Fig. 23, where the delamination lengths versus cycle numbers in logarithmic scale are presented. It can be noted that increasing the maximum load and reducing the load ratio induce a faster propagation of the delamination. Moreover, by plotting the cycle count in logarithmic scale it is seen that after the delamination onset, the delamination growth of all specimens follows an almost linear trend where increasing the load level and reducing the load ratio produces a shift of the curve upwards and decreases the cycle count before collapse occurs.

Inspecting the distribution of the strains at the delamination onset, at the propagation of the delamination to the opposite stringer foot, and at collapse, it was found that these phenomena present similar maximum

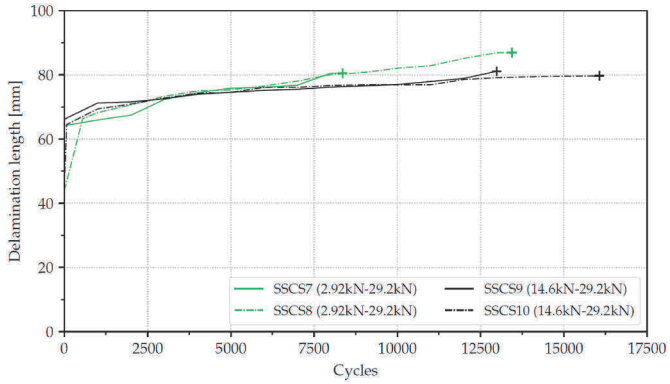

Fig. 22. Delamination length versus cycle count for specimens SSCS7 to SSCS10.

Table 5
Summary of fatigue tests of specimens SSCS7 – SSCS10.

Specimen	Fatigue load [kN]	Load ratio	Delamination onset	Delamination length before collapse [mm]	Collapse [cycles]
SSCS7	29.2–2.92	0.1	28.3 kN	80.5	8358
SSCS8	29.2–2.92	0.1	550 cycles	86.9	13446
SSCS9	29.2–14.6	0.5	28.2 kN	81.1	12987
SSCS10	29.2–14.6	0.5	70 cycles	79.7	16070

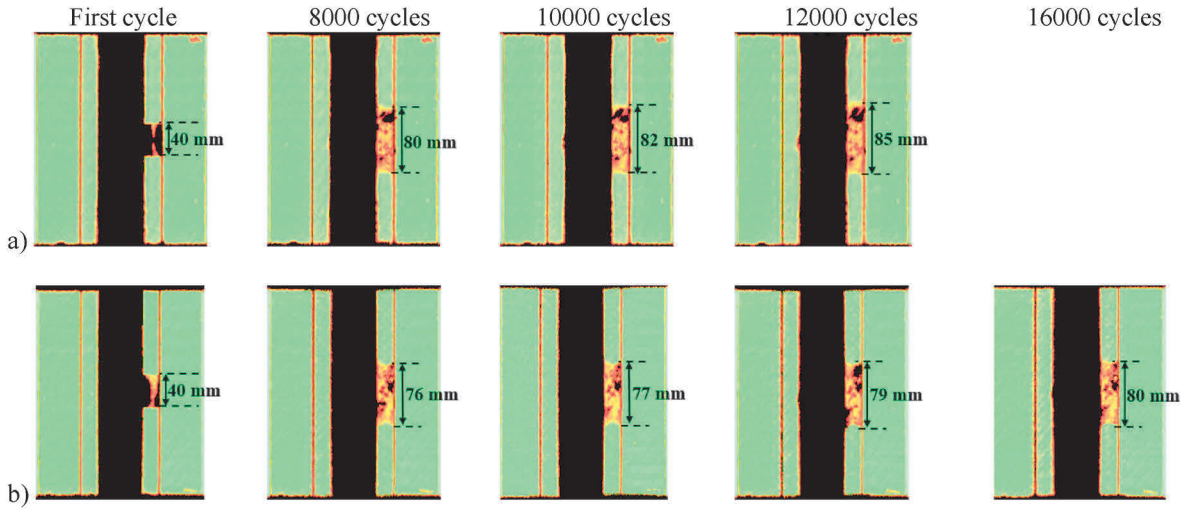

Fig. 21. C-scan during fatigue tests: a) SSCS8; b) SSCS10.

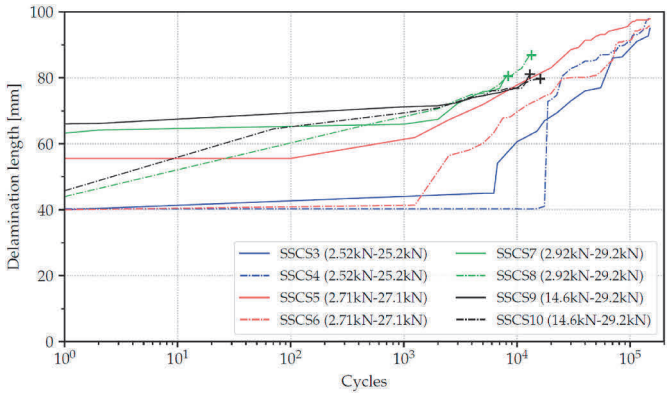

Fig. 23. Delamination length versus cycle count in logarithmic scale for specimens SSCS3 – SSCS10.

strain values at certain locations. These locations are marked in the schematic drawing of the SSCS in Fig. 24 that represents a specimen seen from the skin side, with the stringer feet marked by black dashed lines and the Teflon location shaded in grey. The maximum tension and compression strains along the y-axis are inspected within the dashed blue contour at the delamination onset and at collapse, while the maximum tension strains along the x-axis within the dashed red region are looked into at the propagation of the delamination to the opposite stringer foot.

Table 6 reports the strain values of the outermost skin ply measured by the DIC, and in particular the maximum compression strain along the vertical direction (ε_{yy}) over the initial delamination at the delamination onset, the maximum tension strain along the x-axis (ε_{xx}) at the propagation of the delamination to the opposite stringer foot, and the maximum tension strain on the y-axis (ε_{yy}) over the initial delamination at the collapse.

It can be seen that the maximum absolute strains reached higher values during the quasi-static tests than during the fatigue tests. For specimens SSCS3 – SSCS6, the delamination onset occurred when the maximum compressive strains along the y-axis were on average around

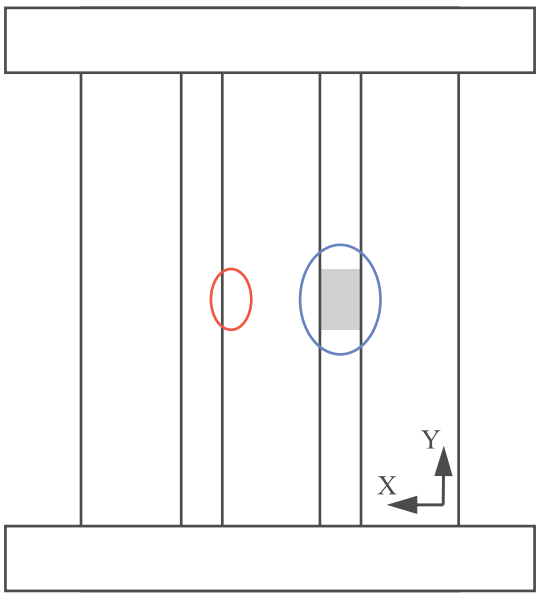

Fig. 24. Schematic of SSCS indicating where strain values are measured before delamination onset and collapse (dashed blue region) and at propagation of delamination to opposite stringer foot (dashed red region). (For interpretation of the references to color in this figure legend, the reader is referred to the Web version of this article.)

Table 6
Maximum strain values at delamination onset, at propagation of delamination to opposite stringer foot, and at collapse.

Specimens	Delamination onset min(ε_{yy}) [$\mu\varepsilon$]	Propagation of delamination max(ε_{xx}) [$\mu\varepsilon$]	Collapse max (ε_{yy}) [$\mu\varepsilon$]
SSCS1	−5320	2630	5780
SSCS2	−5180	2690	5810
SSCS3	−4200	2570	4850
SSCS4	−3750	2650	4650
SSCS5	−4400	2580	4880
SSCS6	−3800	2600	4940
SSCS7	−4400	2130	4020
SSCS8	−4310	2050	4240
SSCS9	−4430	2070	4680
SSCS10	−4610	2100	4620

4000 $\mu\varepsilon$, approximately 20% lower than the values of the quasi-static tests. The strain value and location at the propagation of the delamination to the opposite stringer foot of specimens SSCS3 – SSCS6 were similar to those measured during the quasi-static tests, with maximum tensile strains along the x-axis around 2600 $\mu\varepsilon$. The maximum tensile strains along the y-axis before the collapse were lower and approximately equal to 4900 $\mu\varepsilon$, 15% lower than the average value of 5800 $\mu\varepsilon$ measured during the quasi-static tests. The maximum absolute compressive strains before the delamination onset reached 4400 $\mu\varepsilon$ for SSCS7 and SSCS8, and 4610 $\mu\varepsilon$ for SSCS9 and SSCS10.

The strain values retrieved from the DIC for specimens SSCS7-SSCS10 showed that the maximum tensile strains along the x-axis before the propagation of the delamination to the opposite stringer foot were as low as 2050 $\mu\varepsilon$, 20% lower than the strains measured on specimens SSCS1 and SSCS2, and SSCS3 to SSCS6. This can be attributed to the fact that the propagation of the delamination did not occur during cyclic loading for specimens SSCS1 to SSCS6 but rather during a quasi-static test, which entails that there was little to no degradation of the interlaminar strength at the delamination front due to cyclic loading. For specimens SSCS7 to SSCS10 the delamination propagated under fatigue loads, and the accumulated degradation of the interlaminar strength front resulted in a lower stress threshold before the delamination front propagates to the opposite stringer foot.

Before the collapse, the maximum tensile strain along the y-axis was 4020 and 4240 $\mu\varepsilon$ for SSCS7 and SSCS8, and around 4650 $\mu\varepsilon$ for SSCS9 and SSCS10. The higher values of maximum strains seen in the specimens tested with a load ratio of 0.5 before the delamination onset and collapse suggest that higher stress values can be sustained at the front of the delamination. This occurs due to the slower degradation of the interlaminar strength at the delamination front, thus showing how larger load ratios during cyclic loading induce a slower reduction of the fatigue life for this configuration of stiffened panel.

8. Conclusions

This study experimentally investigated the damage tolerance under quasi-static and fatigue loads in the post-buckling regime of ten single-stringer composite specimens with an initial delamination between one stringer foot and the skin. From the axial compression tests under quasi-static and fatigue loads with different load levels and load ratios, the following conclusions can be drawn for the considered specimen configuration.

- The quasi-static tests showed that the delamination onset, defined when the initial delamination begins growing in length, did not occur until loads approximately twice the buckling load, revealing the large load bearing capacity that stiffened composite panels offer in the post-buckling regime. Collapse occurred at loads over 20% higher than the delamination onset load.

- Fatigue tests in the post-buckling regime with a load level below the delamination onset were conducted for 150000 cycles. The quasi-static tests, performed after the 150000 cycles, showed an average reduction in the collapse load below 10%, when compared to the specimens tested only in quasi-static conditions.
- Fatigue tests with a load level over the delamination onset presented a faster damage propagation and all four specimens collapsed before reaching 16500 cycles.
- Fatigue tests with load ratios equal to R = 0.1 and R = 0.5 showed that delamination lengths increased faster with the lower load ratio due to cycling between pre- and post-buckling conditions. The average number of cycles before collapse for the specimens tested with R = 0.5 was approximately 33% higher than for the specimens tested with R = 0.1.

CRediT author statement

Javier Paz: Methodology, Software, Validation, Investigation, Writing – original draft, Visualization.

Antonio Raimondo: Conceptualization, Methodology, Software, Validation, Investigation, Writing – original draft, Visualization.

Chiara Bisagni: Conceptualization, Methodology, Resources, Writing - Review & Editing, Supervision, Project administration, Funding acquisition.

Declaration of competing interest

The authors declare that they have no known competing financial interests or personal relationships that could have appeared to influence the work reported in this paper.

Data availability

Data will be made available on request.

Acknowledgments

This work was sponsored by the United States Office of Naval Research (ONR), under grant award number N62909-17-1-2129. The views and conclusions contained herein are those of the authors only and should not be interpreted as representing those of ONR, the U.S. Navy or the U.S. Government.

References

[1] Bisagni C, Vescovini R, Dávila CG. Single-stringer compression specimen for the assessment of damage tolerance of postbuckled structures. J Aircraft 2011;48:495–502.
[2] Bisagni C, Dávila CG. Experimental investigation of the postbuckling response and collapse of a single-stringer specimen. Compos Struct 2014;108:493–503.
[3] Kassapoglou C. Design and analysis of composite structures: with applications to aerospace structures. John Wiley & Sons; 2013.
[4] Masood SN, Viswamurthy S, Singh AK, Muthukumar M, Gaddikeri KM. Simulation and validation of disbond growth in co-cured composite skin–stringer specimens using cohesive elements. J Compos Mater 2018;52:807–22.
[5] Krueger R, Paris IL, O'Brien TK, Minguet PJ. Comparison of 2D finite element modeling assumptions with results from 3D analysis for composite skin-stiffener debonding. Compos Struct 2002;57:161–8.
[6] Ouyang T, Sun W, Guan Z, Tan R, Li Z. Experimental study on delamination growth of stiffened composite panels in compression after impact. Compos Struct 2018;206:791–800.
[7] Yap JW, Scott ML, Thomson RS, Hachenberg D. The analysis of skin-to-stiffener debonding in composite aerospace structures. Compos Struct 2002;57:425–35.
[8] Anyfantis KN, Tsouvalis NG. Post buckling progressive failure analysis of composite laminated stiffened panels. Appl Compos Mater 2012;19:219–36.
[9] Paris PC. A rational analytic theory of fatigue. Trend Eng 1961;13:9–14.
[10] Raimondo A, Doesburg S, Bisagni C. Numerical study of quasi-static and fatigue delamination growth in a post-buckled composite stiffened panel. Compos B Eng 2020;182:107589.
[11] Raimondo A, Bisagni C. Analysis of local stress ratio for delamination in composites under fatigue loads. AIAA J 2019;58:455–63.
[12] Dávila C. From S-N to the Paris law with a new mixed-mode cohesive fatigue model for delamination in composites. Theor Appl Fract Mech 2020;106:102499.
[13] Turon A, Bak B, Lindgaard E, Sarrado C, Lund E. Interface elements for fatigue-driven delaminations in advanced composite materials. In: Numerical modelling of failure in advanced composite materials. Woodhead Publishing; 2015. p. 73–91.
[14] Orifici A, Shah S, Herszberg I, Kotler A, Weller T. Failure analysis in postbuckled composite T-sections. Compos Struct 2008;86:146–53.
[15] Dávila CG, Leone FA, Rose CA, Johnston W. Initiation and propagation of skin/stiffener separation in postbuckled structures subjected to cyclic loads. In: AIAA scitech 2021 forum; 2021. 0573.
[16] Raimondo A, Bisagni C. Fatigue analysis of a post-buckled composite single-stringer specimen taking into account the local stress ratio. Compos B Eng 2020;193:108000.
[17] Carreras L, Lindgaard E, Renart J, Bak B, Turon A. An evaluation of mode-decomposed energy release rates for arbitrarily shaped delamination fronts using cohesive elements. Comput Methods Appl Mech Eng 2019;347:218–37.
[18] van Dooren K, Tijs B, Waleson J, Bisagni C. Skin-stringer separation in post-buckling of butt-joint stiffened thermoplastic composite panels. Compos Struct 2023;304:116294.
[19] Degenhardt R, Kling A, Klein H, Hillger W, Goetting HC, Zimmermann R, Rohwer K, Gleiter A. Experiments on buckling and postbuckling of thin-walled CFRP structures using advanced measurement systems. Int J Struct Stabil Dynam 2007;7:337–58.
[20] Abramovich H, Weller T. Repeated buckling and postbuckling behavior of laminated stringer-stiffened composite panels with and without damage. Int J Struct Stabil Dynam 2010;10:807–25.
[21] Cordisco P, Bisagni C. Cyclic buckling tests under combined loading on predamaged composite stiffened boxes. AIAA J 2011;49:1795–807.
[22] Bouslama N, Maslouhi A, Masson P. Experimental and numerical investigation of damage evolution in carbon fiber reinforced polymer stiffened panel in post-buckling regime. J Compos Mater 2022;56:1–16.
[23] da Silva DC, Donadon MV, Arbelo MA. A semi-analytical model for shear buckling analysis of stiffened composite panel with debonding defect. Thin-Walled Struct 2022;171:108636.
[24] Li N, Chen P. Prediction of compression-after-edge-impact (CAEI) behaviour in composite panel stiffened with I-shaped stiffeners. Compos B Eng 2017;110:402–19.
[25] Bai R, Lei Z, Wei X, Tao W, Yan C. Numerical and experimental study of dynamic buckling behavior of a J-stiffened composite panel under in-plane shear. Compos Struct 2017;166:96–103.
[26] Dávila CG, Bisagni C. Fatigue life and damage tolerance of postbuckled composite stiffened structures with initial delamination. Compos Struct 2017;161:73–84.
[27] Dávila CG, Bisagni C. Fatigue life and damage tolerance of postbuckled composite stiffened structures with indentation damage. J Compos Mater 2018;52:931–43.
[28] Raimondo A, Paz J, Bisagni C. Experimental study on post-buckled composite single-stringer specimens with initial delamination under fatigue loads. In: ASC 36TH annual technical virtual conference: composites ingenuity taking on challenges in environment-energy-economy; 2021. p. 418–28.